LABORATORI NAZIONALI DI FRASCATI
SIS – Pubblicazioni

LNF–95/058 (P)
10 Novembre 1995

Polarised and tagged gamma-ray Ladon* beams

D. Babusci[1], M. Capogni[2,3], L. Casano[3], A. D'Angelo[3], F. Ghio[4], B. Girolami[4], L.Hu[3,a], D. Moricciani[3], C. Schaerf[2,3]

[1]INFN - Laboratori Nazionali di Frascati, P.O. Box 13, I–00044 Frascati, Roma, (Italia)
[2]Dipartimento di Fisica, Università di Roma "Tor Vergata", I-00133 Roma (Italia)
[3]INFN - Sezione di Roma 2, Università di Roma "Tor Vergata", I-00133 Roma (Italia)
[4]Istituto Superiore di Sanità and INFN - Sezione Sanità, I-00161 Roma (Italia)

Abstract

The production of polarised and tagged gamma-ray beams by the backscattering of Laser light on the relativistic electrons circulating in storage rings is discussed. The main characteristic and the experimental results of the Ladon and LEGS beams are presented. The Graal beam is introduced.

Submitted to Rivista del Il Nuovo Cimento

---

* Λαδων, "riviere de Grece, au Péloponnèse dans l'Arcadie. ... les Mythologistes firent le Ladon pere de la nymphe Daphné & de la nymphe Syrinx. Il étoit couvert de magnifiques roseaux, dont Pan se servit pour sa flûte á sept tuyaux." (M. Diderot and M. D'Alembert, Encyclopédie, a Paris MDCCLVII).

[a] Now at the Department of Electrical Engineering, Vanderbilt University, Nashville TN 37235.

SUMMARY

1. – HISTORY

In 1963 Arutyunyan and Tumanian [1] and, independently, Milburn [2] have shown that backward scattering of light against high energy electrons could produce high energy gamma-rays. This has been later demonstrated by various authors [3] [4] [5] [6].

In 1967 Malvano, Mancini and Schaerf [7] pointed out that a polarised beam of gamma-rays with an energy and an intensity useful for photonuclear research could be produced by the interaction, in the straight section of a storage ring, of the high electron current circulating in it with the high photon intensity available inside a Laser optical cavity. This was subsequently demonstrated at Frascati on the storage ring Adone where a fully polarised beam of 80 MeV gamma-ray was produced and used for several years for the study of photoreactions [8] [9] [10]. This early success stimulated similar activities in other laboratories. Today Ladon beams are in use in two Laboratories and an higher energy beam is entering into operation:

a. ROKK-1 with a maximum energy of 960 MeV on the storage ring VEPP-4 at Novosibirsk [11];
b. ROKK-2 with a maximum energy of 140 MeV on the storage ring VEPP-3 at Novosibirsk[12];
c. LEGS with a maximum energy of 320 MeV on the X-ray ring at the NSLS in Brookhaven [13] [14];
d. ROKK-1M with a maximum energy of 1600 MeV on the storage ring VEPP-4M in Novosibirsk [15];
e. Graal with a maximum energy of 1500 MeV at the ESRF in Grenoble [16] [17] [18] [19].

The performances of all these beams are summarized in Table I.

Ladon beams are also being considered at CEBAF [20], Duke University [21] and for ELFE, the proposed european electron accelerator.

TABLE I

Project name		Ladon°	Taladon+	ROKK-1	ROKK-2	ROKK-1M	Legs*	Graal**
Location		Frascati			Novosibirsk		BNL	Grenoble
Storage ring Energy defining method		Adone collimation	Adone internal tagging	VEPP-4 tagging	VEPP-3 tagging	VEPP-4M tagging	NSLS external tagging	ESRF internal tagging
Electron enegy	GeV	1.5	1.5		2.0		2.5	6
Photon energy	eV	2.45	2.45	2.34-2.41	2.41-2.53	1.17-4.68	3.53	3.53
Gamma-ray energy	MeV	5-80	35-80	100-960	140-220	100-1600	180-320	350-1500
		variable	s i m u l t a n e o u s					
Energy resolution	%	1.4-10	5		1.5	3	2	1.1
(FWHM)	MeV	0.07-8	4-2	1.5-2	4	10-20	6	16
Electron current	A	0.1	0.1	0.2	0.2		0.2	0.15
Gamma intensity	s^{-1}	10^5	$5 \cdot 10^5$	$2 \cdot 10^5$	$2 \cdot 10^6$	$10^6 - 10^7$	$4 \cdot 10^6$	10^7
Date of operation		1978	1989	1982	1987	1993	1987	1995

° Laser ADONE, +T Agged LADON, * Laser Electron Gamma Source, ** G Renoble A nneau A ccelerateur Laser.

2. COMPTON KINEMATICS

The energy of the photon elastically scattered by a relativistic electron is given by:

$$k = k_1 \frac{1 - \beta \cos\theta_1}{1 - \beta \cos\theta + \frac{k_1}{E}(1 - \cos\theta_2)} \qquad (1)$$

where:

E the energy of the incoming electron,
E' the energy of the scattered electron,
β the velocity of the incoming electron in units of c,
k_1 the energy of the incoming photon,
θ_1 the angle between the direction of the incoming electron and the incoming photon,
θ_2 the angle between the direction of the incoming photon and the scattered photon,
θ the angle between the direction of the incoming electron and the scattered photon

and:

$$z = \frac{4 E k_1}{m^2} \qquad \gamma = \frac{E}{m} \gg 1$$

as indicated in Fig. 1.

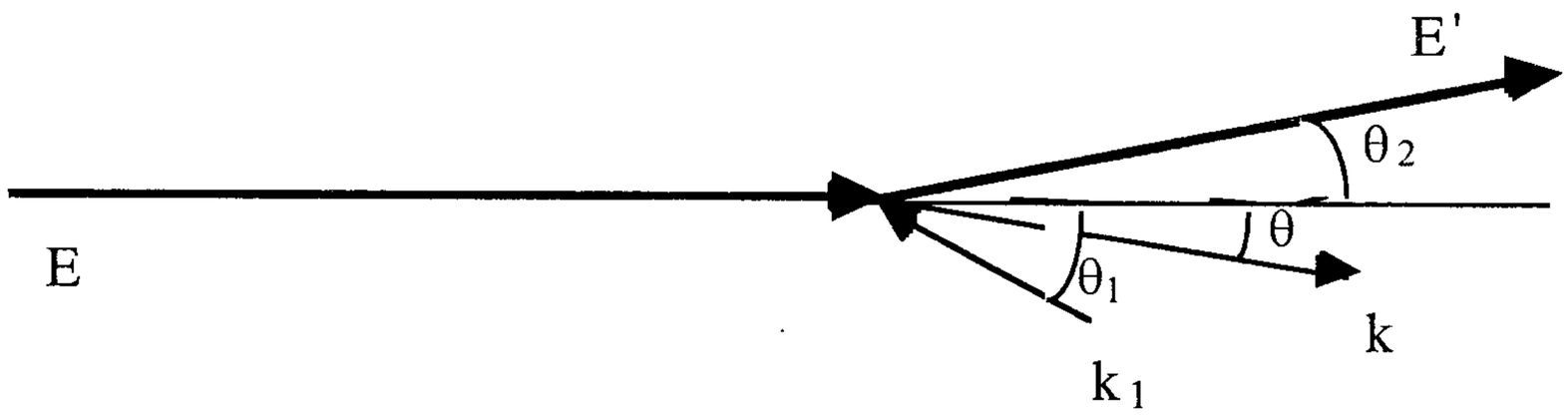

Figure 1 – The kinematics of Compton scattering in flight.

The maximum energy of the scattered photon is given by:

$$k_M = E \frac{z}{1 + z} \qquad (2)$$

or:

$$k_M = \frac{4 k_1 \gamma^2}{1 + z} \qquad (3)$$

which is obtained for 180° scattering in head-on collision on an extremely relativistic electron :

$$ß = 1; \qquad \theta_1 = \theta_2 = \pi; \qquad \theta = 0$$

If:

$$ß \sim 1; \qquad \theta_1 \sim \theta_2 \sim \pi; \qquad \theta \sim 0$$

and

$$x = (\gamma \cdot \theta)^2 \ll 1 \tag{4}$$

Formula (1) becomes:

$$\frac{\Delta k}{k_M} = \frac{k_M - k}{k_M} = \frac{x}{1 + z + x} \approx x \tag{5}$$

If $\Delta\theta$ is the half-aperture of the collimator which defines the gamma-ray beam, then

$$x = (\gamma \cdot \Delta\theta)^2 \tag{6}$$

gives an estimate of the best energy resolution (FWHM) which can be obtained after the collimator.

It is clear from these formulas that defining the energy of the outgoing gamma-ray by its angle requires:

$$x \ll 1 \tag{7}$$

or an angular resolution:

$$\Delta\theta \ll \frac{1}{\gamma} \tag{8}$$

The angle between the electron and the outgoing photon cannot be defined better than the angular divergence of the incoming electron beam. In a storage ring (with small coupling) this is dominated by the angular divergence in the horizontal plane which is indicated by σ'_x. Therefore:

$$\Delta\theta \geq \sigma'_x \tag{9}$$

and we must have:

$$\sigma'_x \ll \frac{1}{\gamma} \tag{10}$$

The energy resolution obtained at Adone in 1979 [10] with the first Ladon beam is reported in Fig. 2 as a function of the primary electron energy and the maximum gamma ray energy. The rise of synchrotron radiation with electron energy increases the beam emittance with deterioration of the gamma-ray energy resolution.

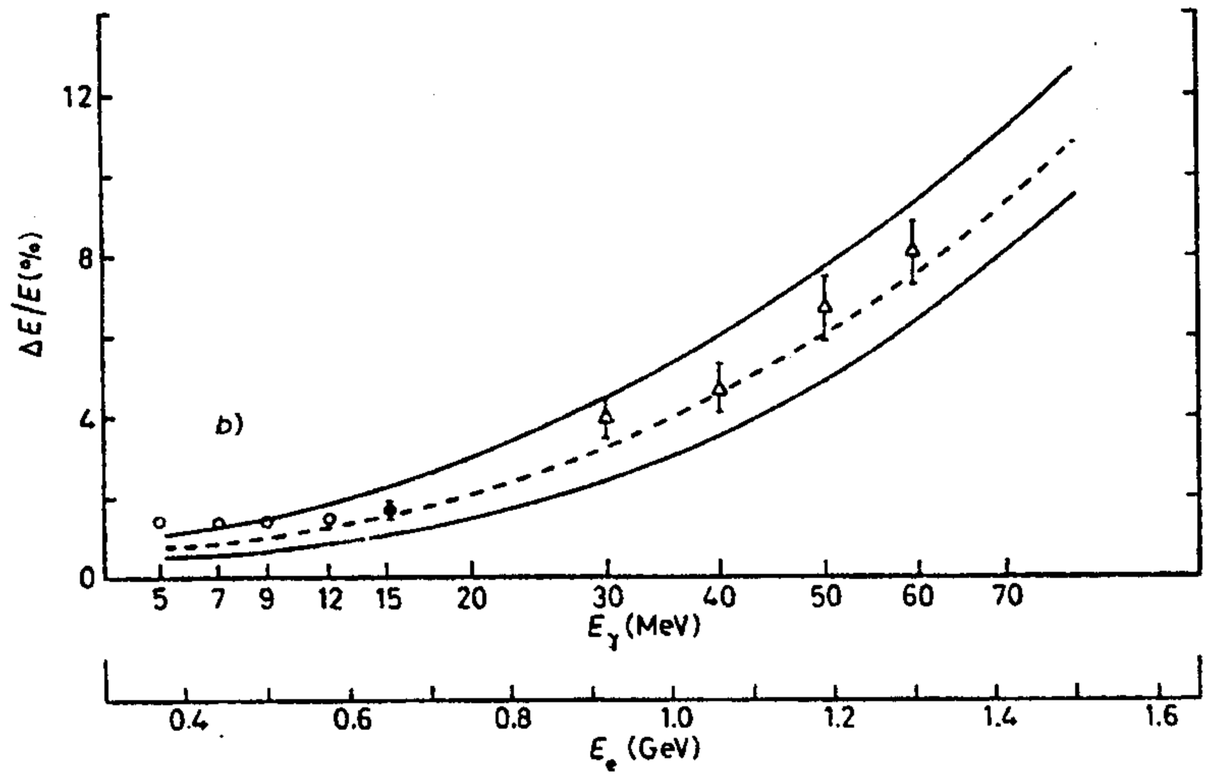

Figure 2 – Fractional energy resolution of the Ladon beam collimated with a solid angle of $2.5 \cdot 10^{-8}$ sr. The dashed lines have been obtained by a Montecarlo calculation with the best estimates available of the electron beam parameters. The solid lines indicate the limits set by our knowledge of these parameters.

3. – YIELD

The total gamma-ray beam intensity is given by the cross section multiplied by 2 c (the relative velocities of electrons and photons in the Laboratory System) and the convolution of the Laser and electron spatial densities:

$$\frac{dn}{dk} = 2\,c\,\frac{d\sigma}{dk}\int u_e\,u_\gamma\,dV \tag{11}$$

or

$$n = 2\,c\,\sigma\int u_e\,u_\gamma\,dV = P\,I\,L \tag{12}$$

where:

$$\sigma = \frac{8}{3}\,\pi\,r_o^2 = 6.6\cdot 10^{-25}\ cm^2 \tag{13}$$

is the classical Thompson cross section, and

n	the total number of gamma-rays per second
$\frac{dn}{dk}$	the total number of gamma-rays per second and per MeV
P	the Laser power in Watt
I	the electron current in Ampere
L	the luminosity in $s^{-1}W^{-1}A^{-1} = W^{-1}\ Q^{-1}$

The luminosity L is obtained by the spatial integration of the photon and electron density distributions. We assume that the Laser and electron beams are perfectly aligned on the z axis and superimposed in the straight section and that their distributions are gaussian in the x and y coordinates (perpendicular to the direction of the beams):

$$u_e = \frac{u_{ue}}{2\ \pi\ \sigma_x\ \sigma_y} \exp\left(-\frac{x^2}{2\sigma_x} - \frac{y^2}{2\sigma_y}\right)$$

$$u_\gamma = \frac{u_{o\gamma}}{\pi\ w^2} \exp\left(-2\frac{x^2+y^2}{w^2}\right)$$

where:

$u_{oe} = \frac{I}{c\ e}$ the electron density on the central trajectory

$u_{o\gamma} = \frac{P}{c\ k_1}$ the photon density on the Laser axis (k_1 in eV)

σ_x the horizontal dispersion of the electron beam

σ_y the vertical dispersion of the electron beam

w the radial dispersion of the Laser beam

e the electron charge

Integrating over x and y we have

$$n = \frac{2\ P\ I\ \sigma}{\pi\ k_1\ e\ c}\ S = 5.5\ \frac{P\ I}{k_1(eV)}\ S \qquad (14)$$

where:

$$S = \int \frac{dz}{\sqrt{w^2(z) + 4\,s_x(z)^2}\ \sqrt{w^2(z) + 4\,s_y(z)^2}} \qquad (15)$$

the integral extended over the lenght of the interaction region.

If the gaussian spatial density distribution of a Laser has a waist in the straight section (of the order of a fraction of a millimetre (rms)), away from this waist its (rms) radius increases according to the formula:

$$w^2(z) = w_o^2\ \left[1 + \left(\frac{z-z_o}{a_o}\right)^2\right] \qquad (16)$$

and

$$a_o = \frac{\pi\ w_o^2}{\lambda} \qquad (17)$$

where:

z	the longitudinal coordinate
z_o	the value of z at the centre of the straight section
w_o	the waist in the centre of the interaction region
λ	the Laser wavelength

The spatial distribution of the electrons is also Gaussian in the coordinates orthogonal to the beam direction. In a magnetic field free region the variances σ_x and σ_y are given by:

$$\sigma_x^2 = \eta^2 \sigma_p^2 + \frac{\varepsilon_o \beta_{ox}}{1 + \kappa} \left[1 + \left(\frac{z-z_o}{\beta_{ox}} \right)^2\right] \tag{18}$$

$$\sigma_y^2 = \frac{\kappa \varepsilon_o \beta_{oy}}{1 + \kappa} \left[1 + \left(\frac{z-z_o}{\beta_{oy}} \right)^2\right] \tag{19}$$

where:

η	the dispersion function, constant along the straight section
σ_p	the rms beam energy spread. Typically: $\approx 10^{-3}$
ε_o	the "natural" beam emittance
κ	the coupling factor between horizontal and vertical betatron oscillations
β_{ox} , β_{oy}	the values of the betatron functions at the centre of the straight section

In a straight section with quadrupoles σ_x and σ_z are given by the values assumed at each point by β_x , β_y and η. The integral S is usually evaluated numerically.

For the Graal project, the ESRF storage ring and the UV lines of an Argon Ion Laser, the result is:

$$L = 2.6 \cdot 10^7 \ s^{-1} A^{-1} W^{-1} \tag{20}$$

Since almost all the scattered electrons are removed from the circulating beam the number of electrons lost per second $(\frac{dN_e}{dt})$ is equal to that of the gamma-rays produced:

$$\frac{dN_e}{dt} = n = L P I = L P N_e e /T = N_e L P e /T = \frac{N_e}{\tau_L}$$

where:

$$\tau_L = \frac{T}{L P e}$$

is the <u>beam mean life</u> produced by the operation of the Laser,

$T = 2.8 \ \mu s$ is the revolution period in the ESRF.

With a Laser power of 4 W (in the UV), now commercially available, we have:

$$\tau_L = \frac{2.8 \cdot 10^{-6}}{2.6 \cdot 10^7 \cdot 4 \cdot 1.6 \cdot 10^{-19}} = 1.7 \cdot 10^5 \ s = 47 \text{ hours} \tag{21}$$

and with a circulating electron current

$$I = 0.15 \text{ A}$$

we have a total gamma-ray flux of

$$n = 1.56 \cdot 10^7 \text{ s}^{-1}$$

which corresponds to a tagged intensity of

$$n_L = 1.04 \cdot 10^7 \text{ s}^{-1} \quad (22)$$

and to a tagged and collimated intensity of

$$N = 0.9 \cdot 10^7 \text{ s}^{-1} \quad (23)$$

Fig. 3 [22] indicates the energy spectrum expected at the ESRF. The upper curve represents the produced beam while the lower curves indicates the spectrum, in the experimental hall, after collimation.

Similar results have been obtained for the Ladon and LEGS beams. They are summarized in Table I.

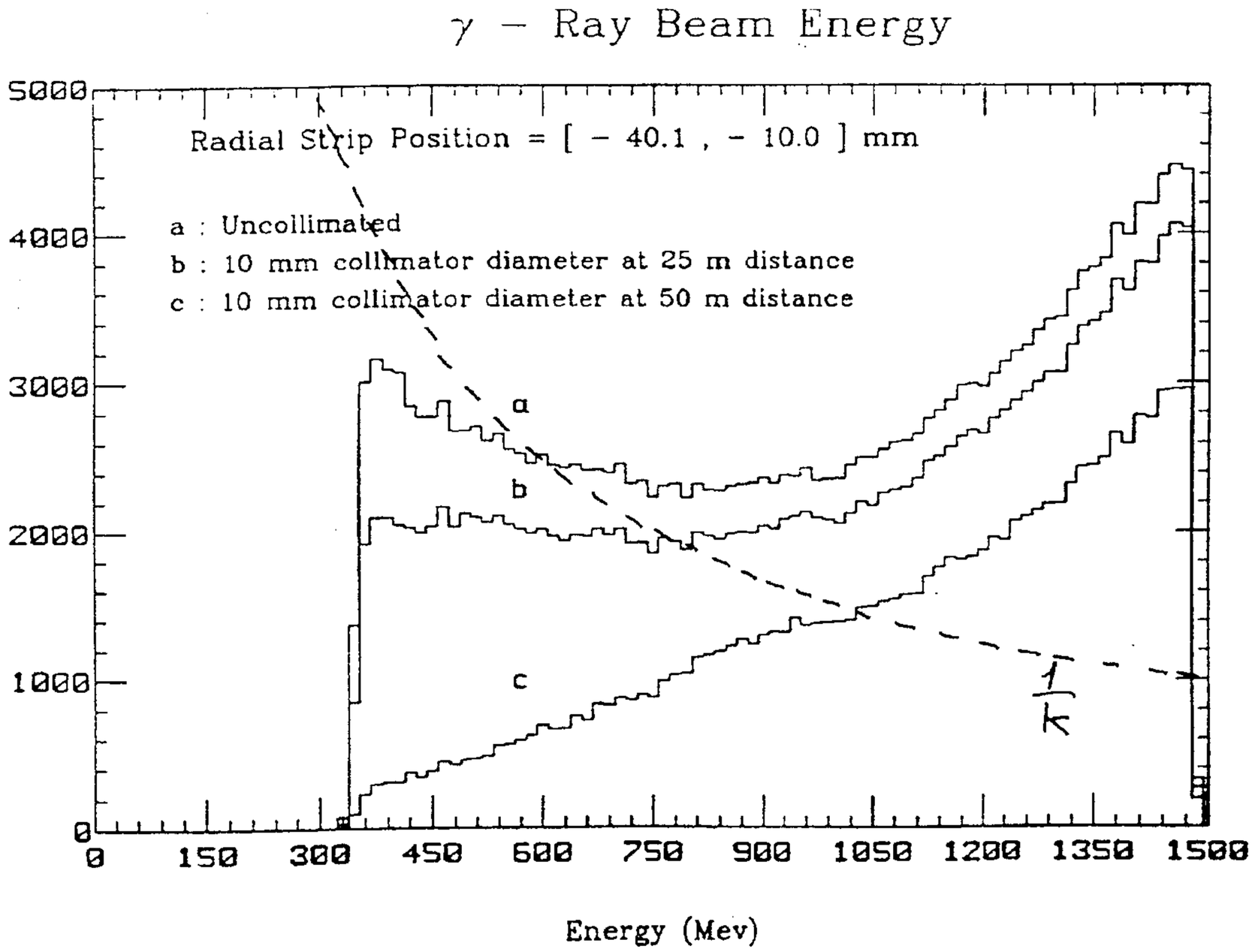

Figure 3 – The energy spectrum of the Graal gamma-ray beam at emission (upper curve) and after a collimation (lower curves). The broken line represents a Bremsstrahlung spectrum: 1/k.

4. – LASER

There are three ways to use a Laser to produce Ladon gamma-ray beams:

1. External Laser power with a short optical resonator;
2. Internal Laser power with a long optical resonator;
3. External Laser power with resonant optical cavity.

4.1 – External Laser power

This is the conventional way to use a Laser. Two mirrors are located at both ends of the plasma tube. A totally reflective mirror at the rear end and a semitransparent one at the front end. The transmission of the latter mirror fixes the fraction of the power inside the resonator which is available on the outside. It also determines the cavity losses (Q) and therefore the power inside the cavity. The transmission of this mirror is chosen by the manifacturer to optimise the output power of the Laser.

In single line operation a prism is placed between the rear mirror and the plasma tube to select the Laser line that one wants to use. In multi-line operation there is no prism and the reflective coating of the mirrors selects a band of lines in the visible or the UV.

The characteristics of the output beam, radius and divergence, are defined by those of the optical resonator: the distance between the two mirrors and their radii of curvature. The distance is slightly larger than the lenght of the plasma tube. The radii of curvature are chosen in such a way as to maximize the power and minimize the emittance of the Laser. To this end the overlap between the Laser energy distribution and the plasma is optimized.

A typical cavity with one plane rear end mirror and a concave front end one is indicated in Fig. 4. It has a waist on the plane mirror given by:

$$w_o^4 = \left(\frac{\lambda}{\pi}\right)^2 d\,(R - d)$$

where:

λ the wavelength of the Laser
d the distance between the mirrors
R the radius of curvature of the concave mirror

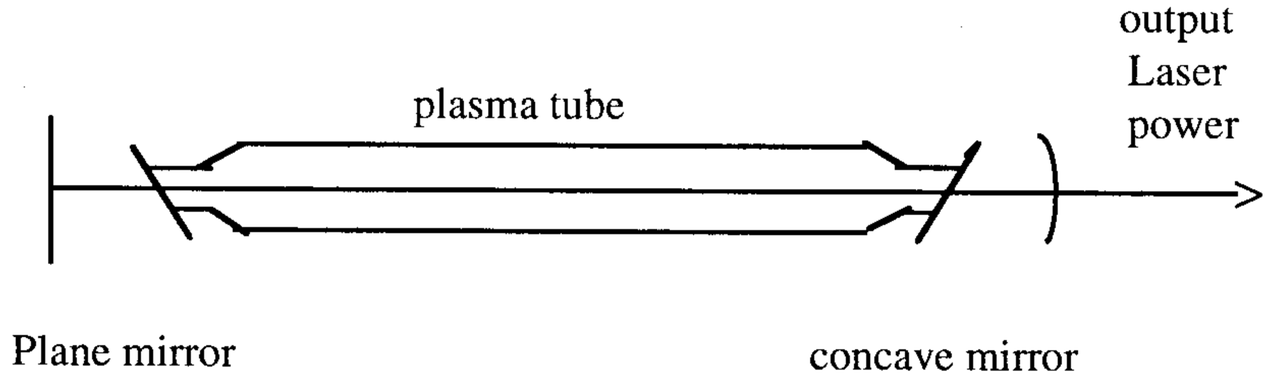

Figure 4 – Typical Laser resonator with one plane and one concave mirror.

The plasma tube has two Brewster windows at each end. They are used to minimise intracavity losses and define the plane of polarisation of the light. The Laser power available for the experiment is that indicated by the manufacturer.

4.2 – Internal Laser power

In the previous configuration the power inside the Laser cavity between the mirrors is usually an order of magnitude higher than the power available outside since the trasmission of the output mirror is typically between 5 and 10 percent. Therefore to obtain a higher gamma-ray flux it has been suggested to use the power inside the cavity. Moreover this power can be increased using mirrors totally reflective to reduce the cavity losses. In this configuration the Laser-electron interaction region must be inside the Laser optical resonator and the Laser cavity must overlap the straight section of the storage ring. This technique was successfully employed in the Ladon beam at Frascati [10] with an optical resonator schematically indicated in Fig. 5.

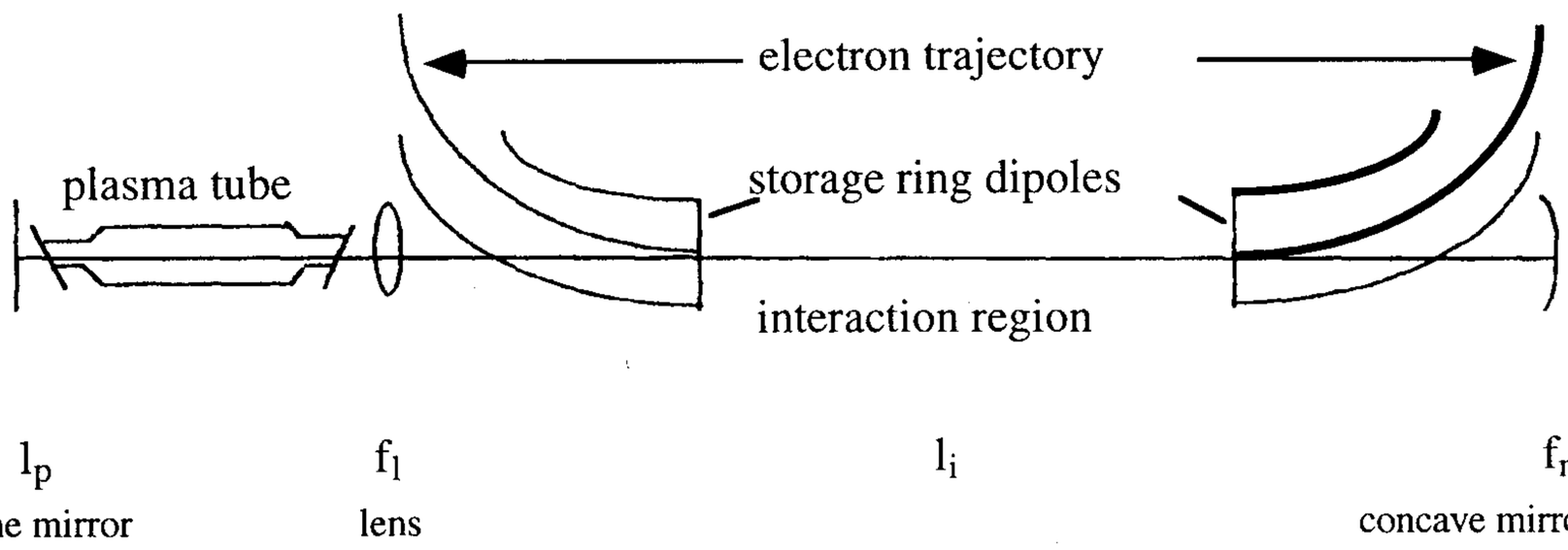

Figure 5 – Long Laser resonator with three optical components. Both mirrors are totally reflecting and the lens has antireflection coating. To the right of the lens the Laser photons enter the ring vacuum chamber. The electron-Laser interaction takes place between the two magnetic dipoles where the Laser and electrons are superimposed.

This set up has four free parameters:

l_p the distance between the plane mirror and the lens whose minimum value is fixed by the length of the plasma tube ($\approx$ 2 m);

l_i the distance between the lens and the concave mirror whose minimum value ($\approx$ 15 m) is determined by the length of the straight section and the dimensions of the storage ring magnetic dipoles;

f_l the focal length of the lens;

f_m the focal length of the concave mirror.

The parameters are adjusted to produce two waists: one on the plane mirror and the second in the interaction region. The first one is set similar to the one selected by the Laser manifacturer for the conventional configuration. The size of the second waist is chosen to optimize the value of the integral S in Eq. (15) and therefore the luminosity. The position of the waist defines the interval of z were the photon density is maximum and therefore there is the

maximum production of gamma-rays. Its position, in the interaction region, is used to find the best compromise between the luminosity and the gamma-ray energy resolution. The introduction of a second lens, at some distance from the first one, will introduce two more degrees of freedom, its focal length and the distance between the lenses, and therefore more options in the design of the system.

4.3 – External Laser power with resonant optical cavity

This possibility is discussed extensively in reference [20].

4.4 – The Ladon Optical system

Fig. 6 indicates the set up used in the Ladon beam. Two additional mirrors are used to rise the beam in the vertical plane, to align the Laser cavity and to superimpose its axis with the electron beam. The lens acted also as vacuum window to enter the light into the accelerator vacuum chamber. The concave mirror was in vacuum.

The gain in power which can be obtained using the power inside the laser cavity is very large, of the order of Q, the quality factor of the cavity, since this is the average number of times a photon travels in the cavity before is lost. In priciple Q can be made very large reducing the cavity losses with high quality optics. In practice the major limiting factor is the damage inflicted on the lenses and mirrors by the sinchrotron radiation emitted by the electrons in the storage ring. Ladon runs were usually two weeks long. Optical components were cleaned or changed before the runs.

We started with about 80 W of Laser power which decreased to about 50 W in a few hours. After that a slow decline set in. The power after two weeks of running was between 30 and 40 W.

The stability in the position of the optical components is also critical. In our case they were all remotely controlled by an old PDP11/04 computer which automatically searched for the maximum Laser power moving the two alignement mirros and the concave mirror at the end of the cavity. This took about an hour. During the injections in the ring a more limited programme was used to optimise the cavity moving only the concave mirror. This yielded a gain of few tens of percent. The deterioration of the lens and the concave mirror was manifest by the formation of a small black film on their surface in the spot presumably irradiated by synchrotron radiation. It is not clear if the optimisations done at injections improved the alignement of the cavity or selected a cleaner part on the mirror and the lens.

No systematic study was made of the deterioration of the optical components. It increased with the energy and current of the electron beam and therefore the amount of synchrotron radiation emitted. But it was also dependent on the pressure of the residual gas in the vacuum chamber. After an opening of the ring, when the vacuum inside it was poorer, the decrease of Laser power was more rapid. At LEGS, were the amount of synchrotron radiation is larger, but the machine vacuum is much better, the degradation of the optical components is much slower.

A possible interpretation of the phenomenon is that synchrotron radiation cracks the molecules of residual gas and that the Carbon contained in many of them sticks to the surface hit by the radiation. Chemical analysis indicated that Carbon was the main component of the black spots.

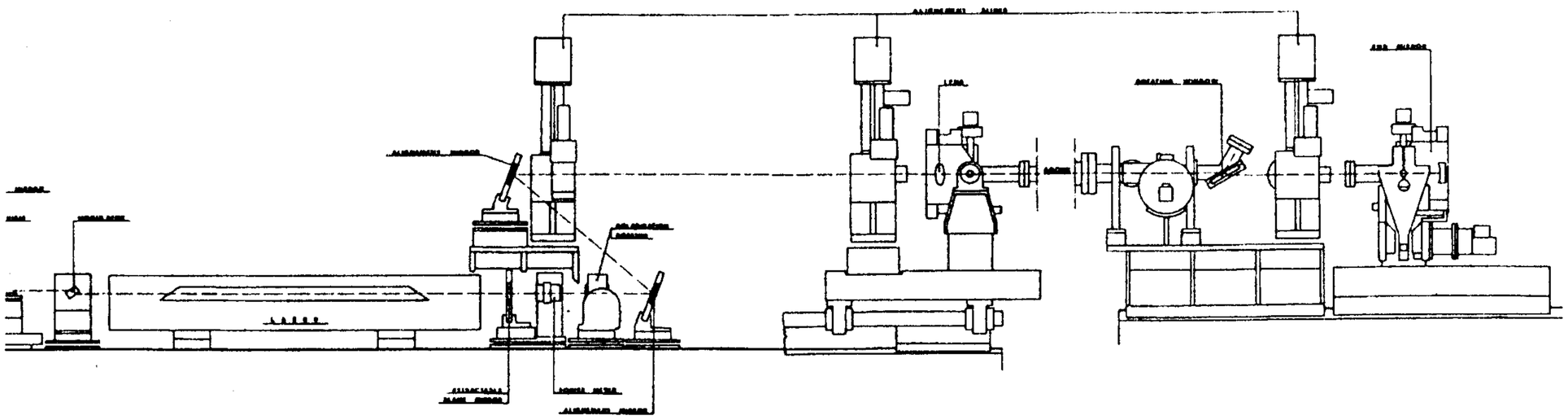

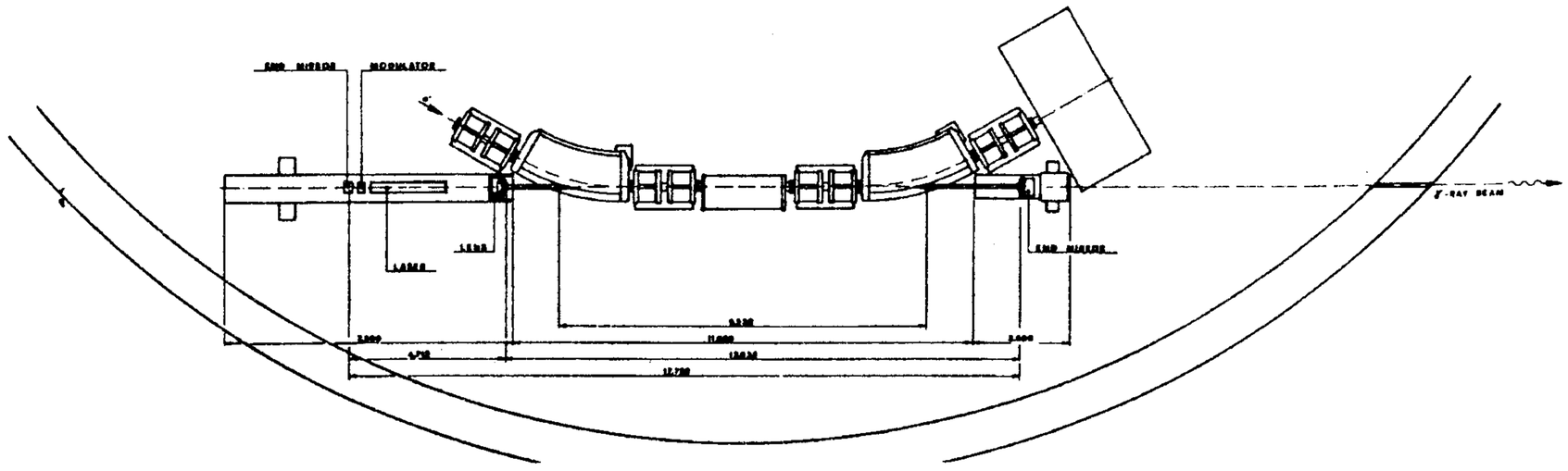

Figure 6 – Schematic view of the installation of the Laser cavity on the storage ring Adone.

4.5 – The LEGS and the Graal optical systems

In the LEGS and Graal projects the maximum amount of gamma-rays which can be extracted is fixed by the limits set by the management of the rings on the minimum beam lifetime introduced by the Lasers. In these cases the external power (5÷10 W) provided by commercially available Laser is enough and there is no need to go into the complications of long cavities and internal power.

The Graal optical system is indicated in Fig. 7. It consists of three lenses, pratically a zoom, to change the size of the waist and its position along the interaction region. The totally reflecting plane mirror at the rear and the semitransparent concave mirror are those provided by the Laser manifacturer. Not indicated in this drawing are an optional prism between the plasma tube and the plane mirror used for single line operation and a periscope between the second and third lens used to bring the light from the height of the Laser to the height of the electron ring. The double prism parallele translator and the Be mirror are used for the precision alignement of the Laser on the electron beam. Beryllium is used for its low Z which reduces the absorption of gamma-rays.

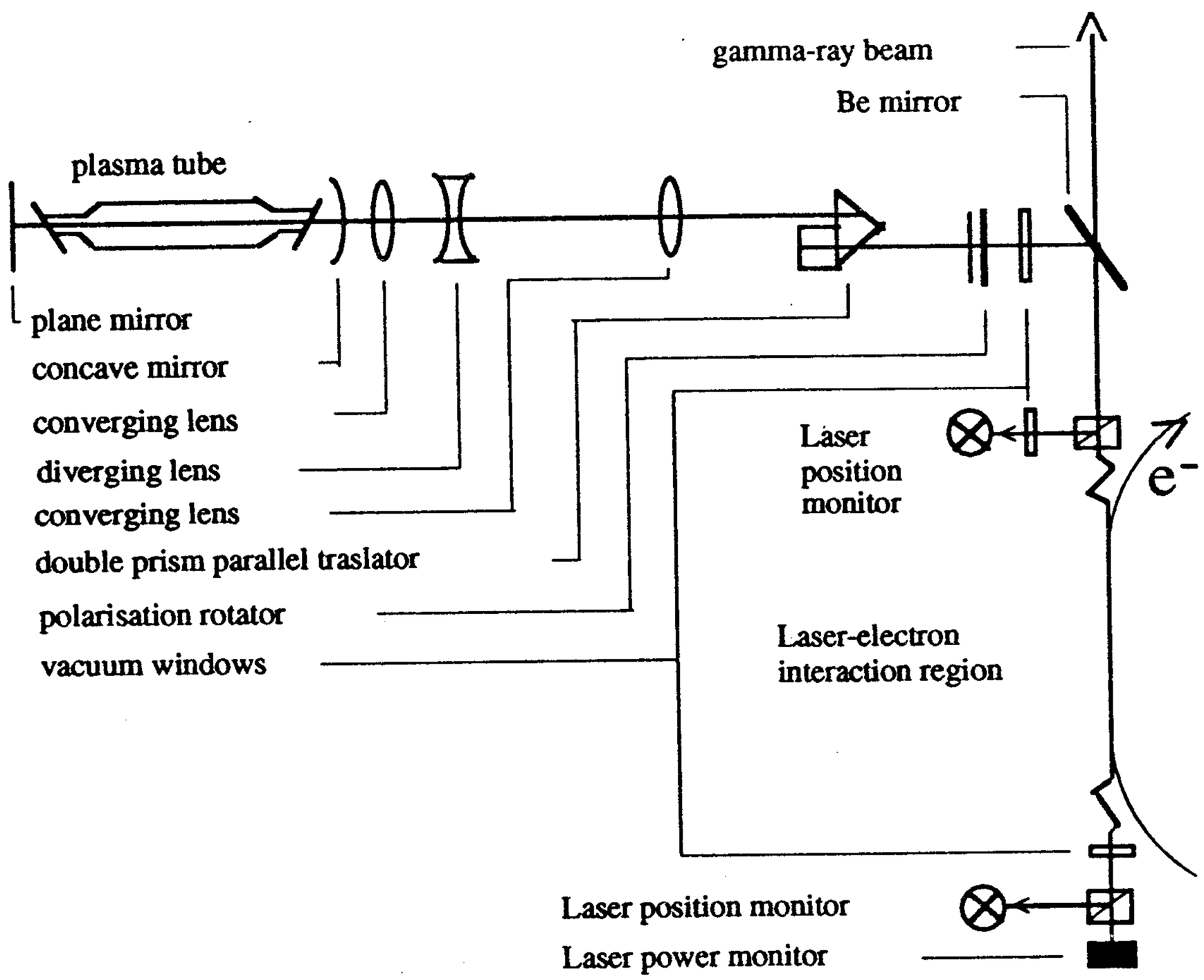

Figure 7 – The optical set up of the Graal beam. The Beryllium mirror and the double prism are used for the precision alignement of the the Laser light on the electron beam. The three lens zoom is used to adjust the size and longitudinal position of the Laser waist.

5. – TAGGING

At an electron energy above 2 GeV it is difficult to achieve condition (10). Therefore to define the gamma-ray energy we tag the final electron.

The energy of the scattered gamma-ray is also given by:

$$k = E - E' + k_1 \cong E - E' \tag{24}$$

Therefore if we know the energy of the initial electron and we measure the energy of the final one we can determine the photon energy with an error (rms) given by:

$$\sigma_k^2 = \sigma_E^2 + \sigma_{E'}^2 \tag{25}$$

where σ_E and $\sigma_{E'}$ are the rms energy resolutions of the incident and scattered electrons and are correlated if we work in a dispersive section of the storage ring.

The energy dispersion of the initial electron is determined by the characteristics of the storage ring. In a ring of modern design with enough damping it is given by:

$$\sigma_E = \sigma_p E \approx 10^{-3} E \tag{26}$$

To measure the energy of the final electron with enough resolution we must use a magnetic spectrometer and a detector system that correlates in time (tag) the reaction produced by the gamma-ray with the electron which has scattered it.

Two types of tagging have been built and operated: internal and external.

In internal tagging the scattered electrons are momentum analysed by the magnets and quadrupoles of the storage ring. Since the storage ring lattice is usually designed for low magnetic dispersion, the tagging counters must be located very close to the main orbit of the storage ring. In Adone they had to be remotely removed during injection to protect them from the radiation damage of stray electrons and to free the entire vacuum chamber for the injected particles.

In external tagging the scattered electrons are removed from the machine lattice with the help of an auxiliary magnetic field located after the first dipole, and are momentum analysed by an external magnetic spectrometer. The auxiliary magnet must be trimmed very carefully to produce a field of less than one Gauss on the main orbit in order not to disturb the circulating electrons.

With respect to the most important parameter, which is the gamma-ray energy resolution, the calculated performances of both systems are comparable in the sense that both can approach the limit imposed by the electron beam properties.

Their main differences are:

1. internal tagging is less expensive to build and operate because it does not require new magnets and does not increase the volume of the vacuum chamber by an appreciable amount;

2. since a detector can be located closer to the main orbit than a magnetic field can, internal tagging sets a lower limit on the minimum gamma-ray energy that can be tagged and therefore yields, ceteris paribus, a higher gamma-ray intensity;
3. in internal tagging the detectors must have a high spatial resolution (dx < 1 mm) and must therefore be Microstrip solid state Silicon Detectors (μSD) or scintillating optical fibres. Being very close to the beam they will suffer radiation damage and, in particular the microstrips, will have to be replaced periodically: at Adone they lasted for more then a year but were held several centimetres above the plane of the beam orbit when the Ladon beam was not in operation.
4. in external tagging the detectors do not need very high spatial resolution (dx ≈ 10 mm) and can therefore be made out of more stable plastic scintillators. They can be located at a reasonable distance from the ring in a radiation-safe location which could be accessible during operation of the ring.

5.1 Internal tagging

The energy resolution of an internally tagged Ladon beam has been derived by M. Preger[17] in the linear approximation:

$$\sigma_k = E\,\sigma_{xT} / d \qquad (27)$$

where

$$\sigma^2_{x\,T} = \varepsilon_x \beta_{xT} + \eta^2_T\ \sigma^2_P$$

and

d is the energy dispersion of the magnetic components of the ring lattice from the interaction region to the tagging detectors (A_{13} in many matrix notations) [m];
ε_x is the horizontal emittance of the stored beam [m · rad];
σ_P is the fractional energy spread of the stored beam;
β_{xT} is the horizontal betatron wave-length at the position of the tagging detectors [m];
η_T is the energy dispersion at the tagger [m];

ε_x and σ_P are global machine parameters, β_{xT} and η_T depend on the position of the tagging detectors, while d depends on the positions of the interaction region and the tagging detectors.

Practically, on each storage ring, there is only a very limited choice for the positions of the interaction region and the tagging detectors. At the NSLS and the ESRF, and other machines with a Chasman Green lattice [23] there are two types of straight section and therefore one can choose in which one to locate the interaction region, but Adone had only one type of straight section.

The gamma-rays with the highest energy and the highest polarisation are associated with the electrons which have lost the largest fraction of their energy. After the first dipole these electrons will drift inward and will eventually hit the walls of the vacuum chamber. The tagging detector must be located before this happens and therefore shortly after the first dipole. At the ESRF it is located directly after the dipole.

5.1.1 – The Ladon beam at Adone

Numerical results for Adone were first estimated using a Montecarlo simulation [24] which followed the trajectories of the scattered electrons in the storage ring magnetic lattice from the interaction to the tagging region. These results have also allowed the identification of 0.55 mm as the maximum pitch of the tagging counters which does not appreciably affect the energy resolution. The basic cell of Adone (1/12 of the storage ring) consists of one dipole with two quadrupoles on each side as indicated in Fig. 8.

The tagging counters were located after the first quadrupole in the straight section following the interaction region (position A in Fig. 8). They consisted of a solid state microstrip detector (μSD) built on a silicon wafer 0.3 mm thick and composed of 96 vertical strips with a pitch of 0.55 mm. Behind it was located a fast plastic scintillator viewed by a photomultiplier as shown in Fig. 9.

The signal of each microstrip went through a fast preamplifier, amplifier and entered a discriminator strobed by the scintillation counter. The outputs of the discriminators were fed to 96 channels of CAMAC input registers synchronised with an event in the experimental apparatus.

In the experimental hall, 50 meters from the interaction region, the beam passed a collimator, a pair spectrometer, the experimental apparati and finally entered a large NaI crystal. The NaI(Tl) monitored the intensity of the gamma-ray beam while the magnetic pair spectrometer[25] was used to measure its spectrum. The pair spectrometer bent the electrons and positrons by 180° into a wire chamber system and two pairs of plastic scintillators. The positions of the particles in the wire chambers were related to their energies and their combined values gave the gamma-ray energy with an error of less then 1%.

Correlating the microstrip input registers and the wire chamber readout system it was possible to obtain one gamma-ray spectrum for each microstrip. In Fig. 10 we have indicated a sample of these spectra: one every five microstrips.

The most interesting results are the narrow width of the peaks at the highest energies and the double peak at intermediate energies. This is due to the fact that in the experimental hall the beam passes through a collimator with a bore of 8 mm diameter which defines an half aperture angle at the source (the interaction region) of $8.9 \cdot 10^{-5}$ rad. Since the gamma rays with the highest energy are emitted at a very small angle ($< 10^{-4}$ rad) from the direction of the incident electrons, only those electrons which have a small angular divergence can radiate an high energy photon which enters our very small collimator. In this way our apparatus selects a subset of electrons with a smaller angular divergence than average.

The elements of the transport matrix of the Adone magnetic lattice from the interaction region to the tagging counters are:

$a_{11} = (x|x_o) = 0.125 \ll 1$
$a_{12} = (x|x'_o) = 7.60$ m
$d = a_{13} = (x|\delta) = 1.41$ m

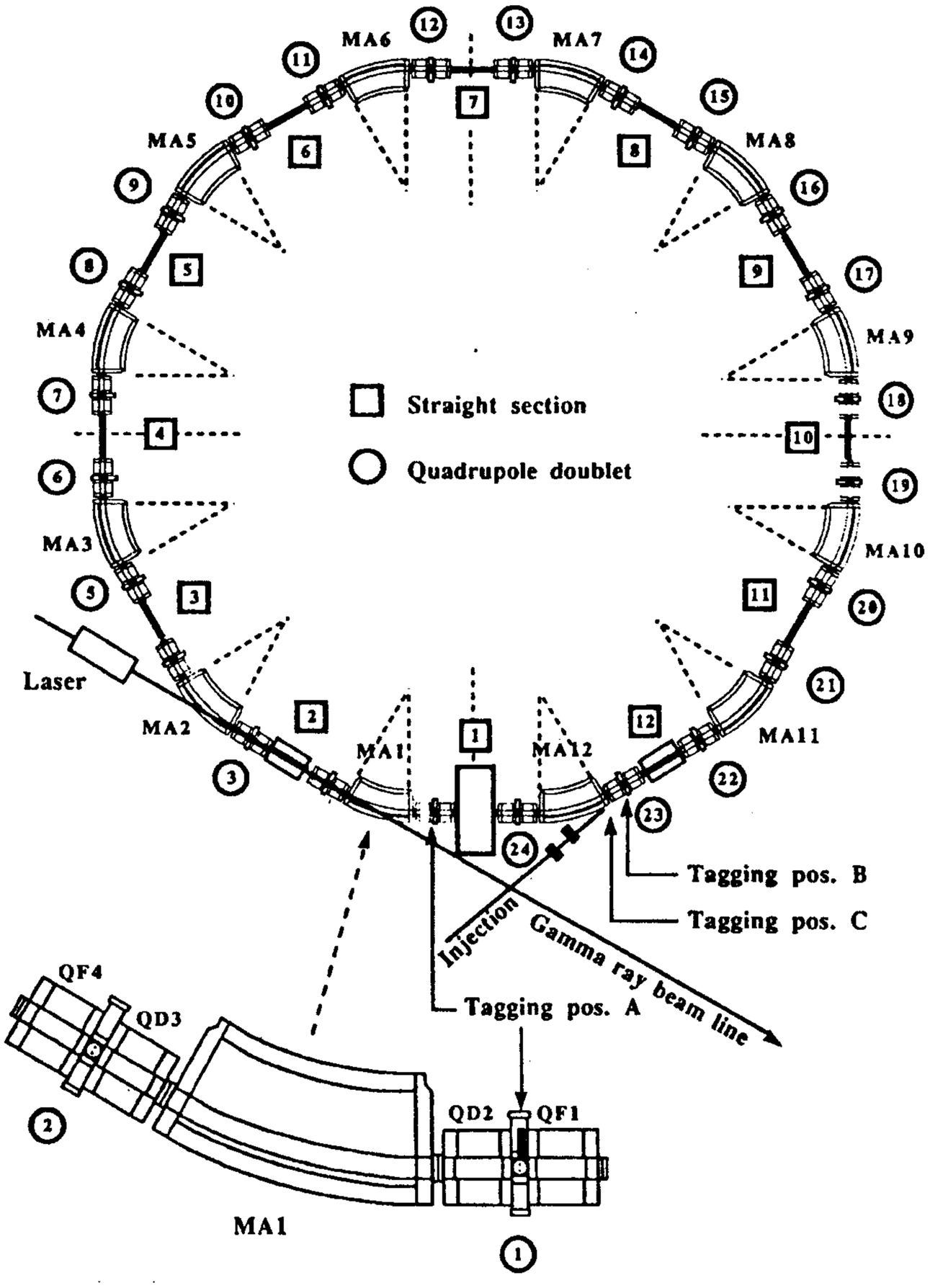

Figure 8 – A schematic representation of the layout of the Adone storage ring with an indication of the electron-Laser interaction region, the position (A) of the tagging counters and the direction of the gamma-ray beam.

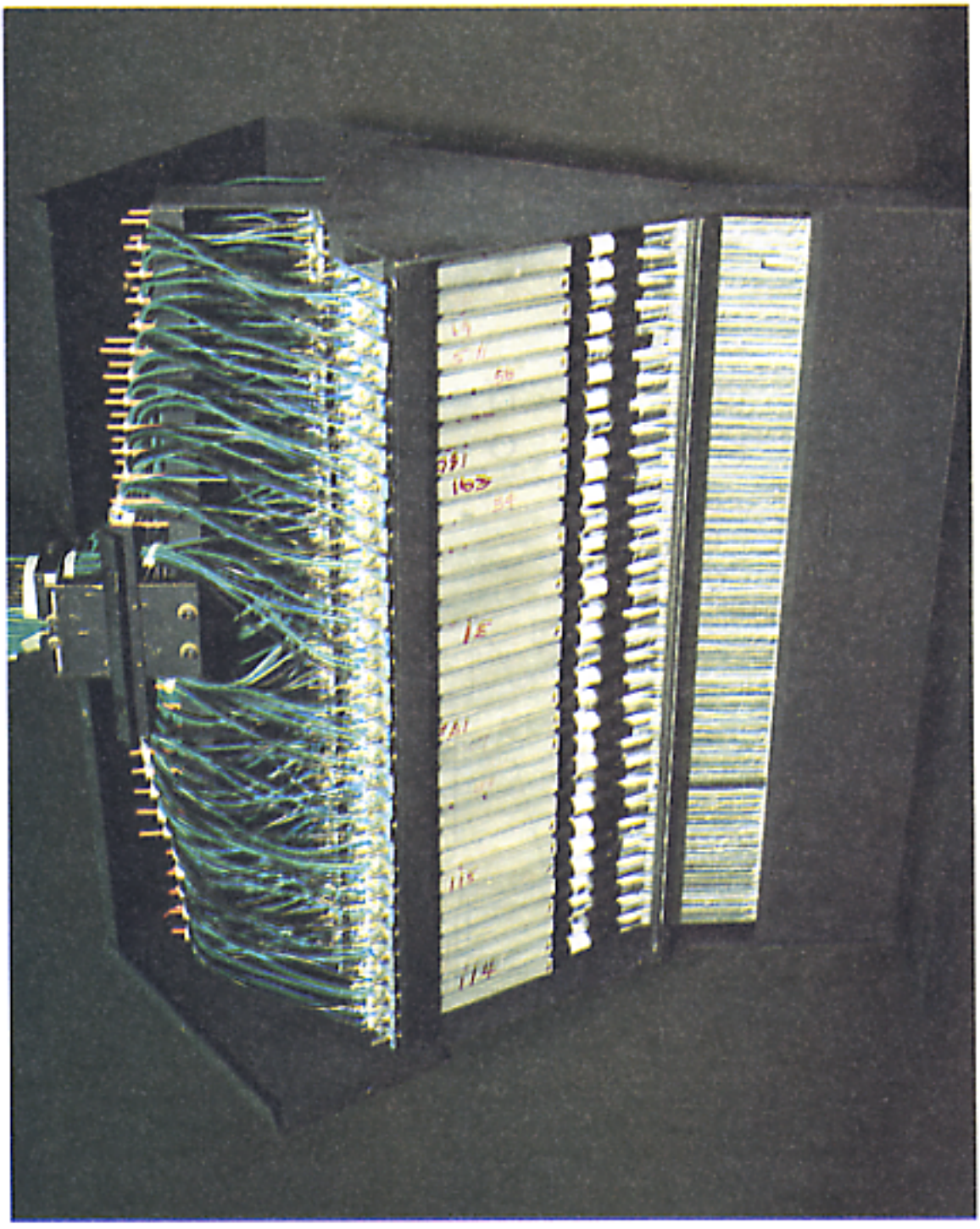

Figure 9 – The tagging detector system of the Ladon beam at Frascati.

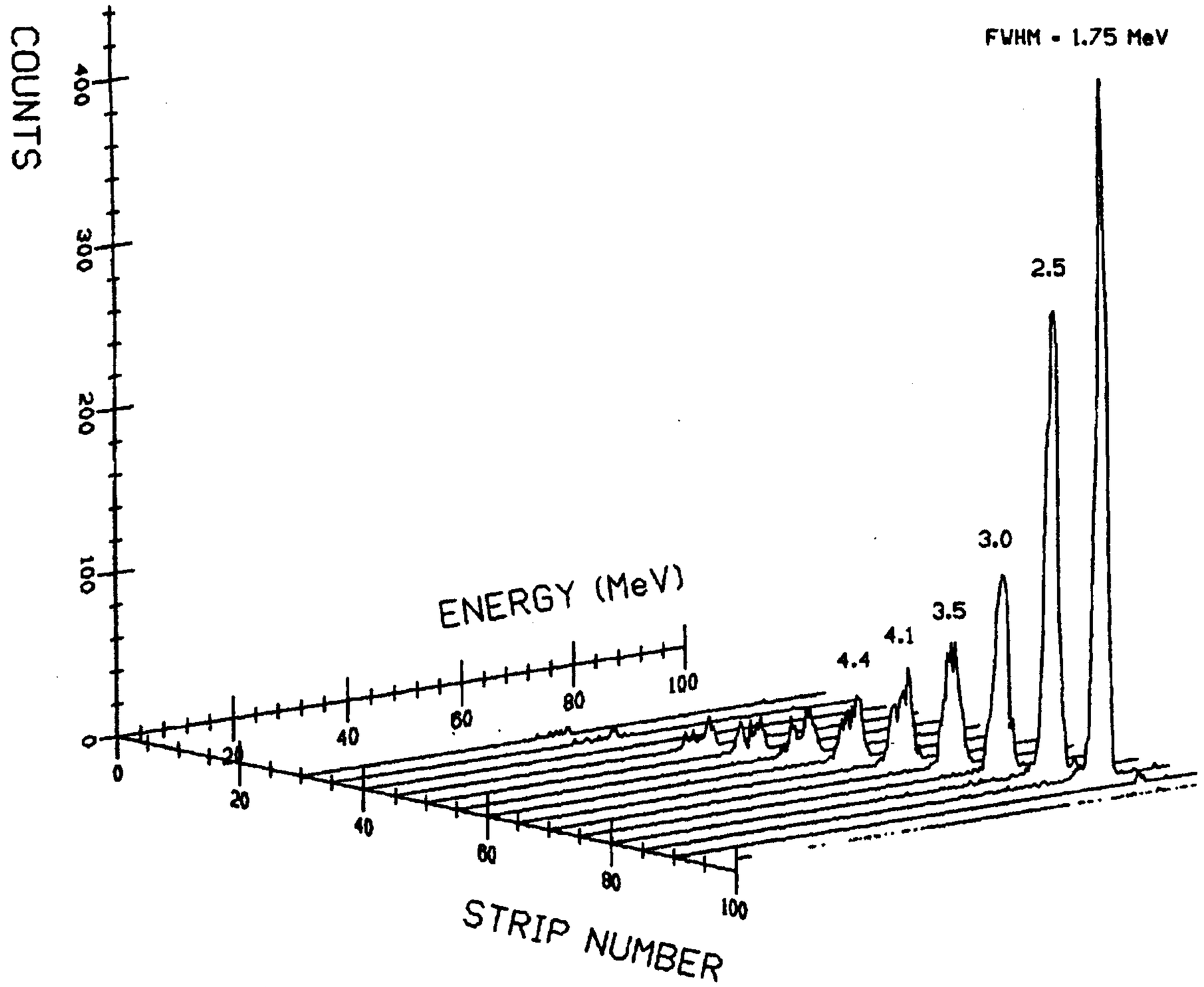

Figure 10 – Gamma-ray spectra measured by the magnetic pair spectrometer in coincidence with selected microstrips.

The distance from the equilibrium orbit of an electron at the tagger as a function of its canonical coordinates in the interaction region is given by:

$$\Delta x \cong a_{11}\,\Delta x_o + a_{12}\,\Delta x'_o + a_{13}\,\delta \cong a_{12}\,\Delta x'_o + a_{13}\,\delta$$

where

$$\delta = \Delta E/E = \Delta k/E$$

is the quantity of interest and the main source of error is:

$$a_{12}\,\Delta x'_o \approx 7.6 \cdot 8.9 \cdot 10^{-5} \approx 6.8 \cdot 10^{-4}\ \mathrm{m}$$

Therefore a smaller electron angle x'_o will produce an improved energy resolution:

$$\frac{\Delta k}{E} \approx \frac{a_{12}\,\Delta x'_o}{d}$$

and

$$\Delta k = 1500 \cdot 6.8 \cdot 10^{-4} / 1.41 = 0.72 \text{ MeV (rms)}$$

which is equivalent to a Full Width at Half Maximum (FWHM) of:

$$\Delta k_{model} = 1.7 \text{ MeV}$$

a value in good agreement with our experimental result of:

$$\Delta k_{experimental} = 1.75 \text{ MeV}$$

While the value given by formula 27 for the uncollimated beam is:

$$\Delta k_{theory} = 4 \text{ MeV}$$

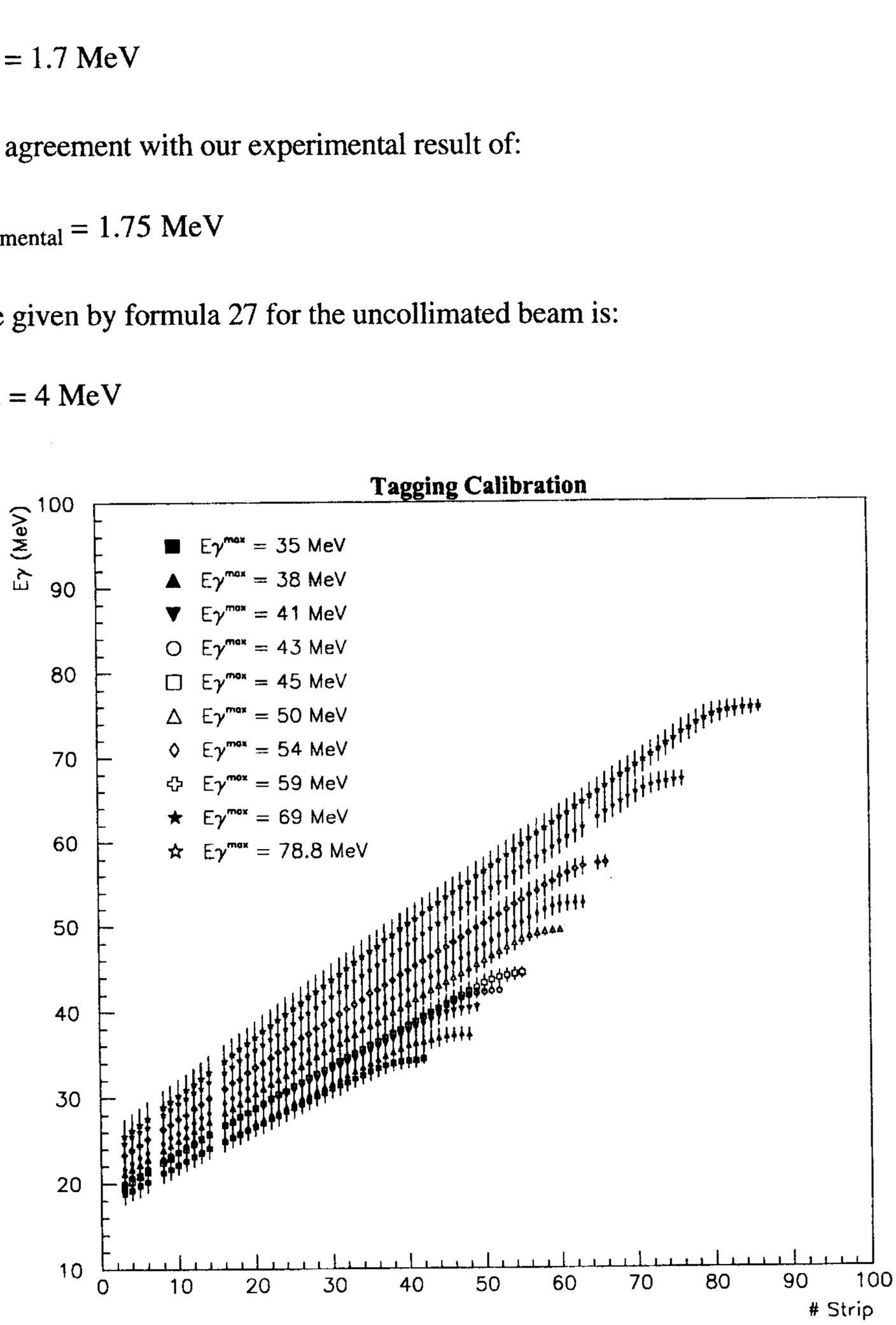

Figure 11 – Energy calibration of the tagging detector for different values of the maximum gamma-ray energy.

Similar arguments can be used to explain the two-peak structure if we remember that gamma rays of intermediate energy are emitted at an angle with respect to the direction of the electron.

The energy calibration of the tagging detector and its energy resolution, for different values of the primary electron energy and the maximum photon energy, are indicated in Fig. 11 and 12.

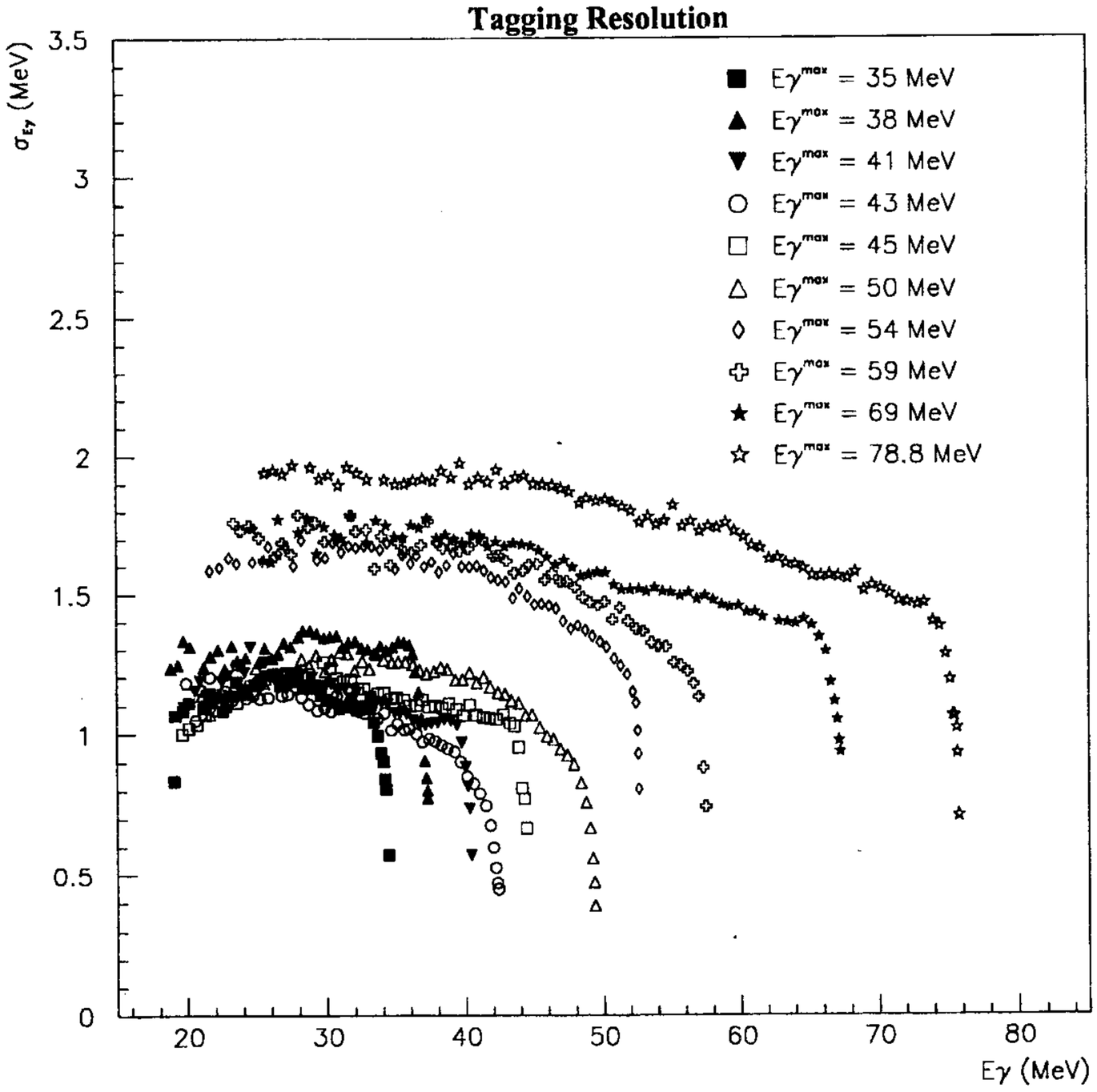

Figure 12 – Energy resolution of the tagging detector for different values of the maximum gamma-ray energy.

5.1.2 – The Graal beam at the ESRF

The present magnetic lattice of the ESRF is indicated in Fig. 13. It is very similar to the one published in the ESRF red book [26]. It alternates short and long straight sections. The long ones are dispersion free and are dedicated to insertion devices like wigglers or undulators. Those dedicated to wigglers have low beta in the centre to obtain a very small beam, while those for undulators have high beta for a highly parallel beam. The short straight sections have a small dispersion in the centre of the order of 0.5 m.

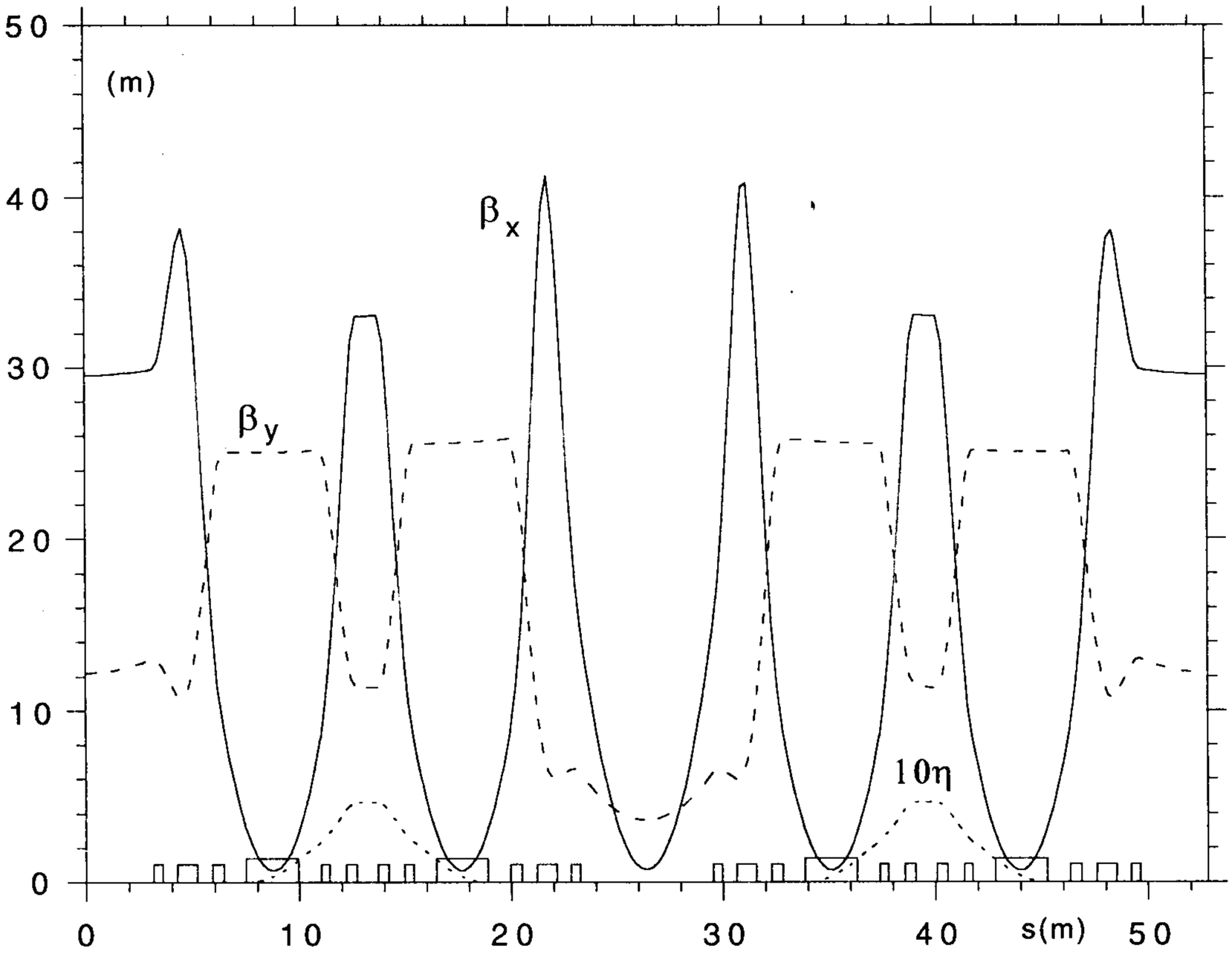

Figure 13 – The basic cell of the ESRF (1/16 of the ring) and its associated optical functions. The origin is in the centre of an undulator straight section

The Graal facility is installed on the short section corresponding to exit port D7 to take advantage of the extra space available there in the experimental hall since the preceeding long straight section is occupied by the injector and its exit port (ID6) is not available for experiments.

Fig. 14 indicates the dispersion d calculated, in the linear approximation, from the centre of the interaction region and the ratio σ_{xT} / d which provides a first estimate of the energy resolution.

The dispersion curve shows that electrons which have lost 1.8 GeV will hit the vacuum chamber after exiting the first dipole and before entering the following quadrupole. Therefore the main tagger must be located in this region and can cover a gamma-ray energy region between 400 and 1800 MeV. The lower energy region (from pion threshold to the Δ_{33} resonance) could be covered with another tagger located in centre of the straight section between the third and the fourth quadrupole.

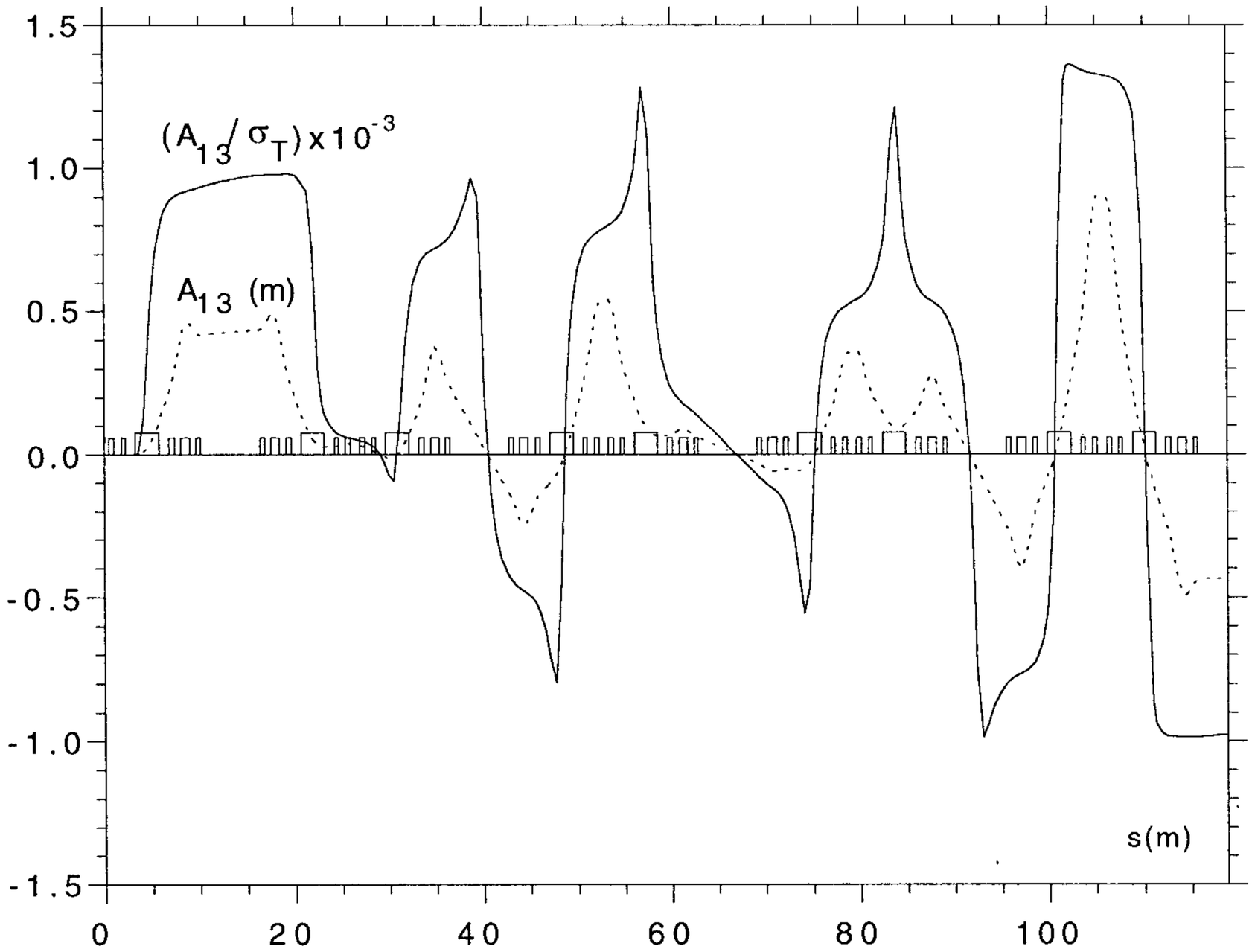

Figure 14 – Dispersion and energy resolution at the ESRF as a function of the position of the tagger, calculated from the centre of a short straight section.

The early calculations done at Frascati [16] [17] [18] to estimate the yield and energy resolution of the Graal beam have been later repeated at the ISN in Grenoble [19] taking into account also second order corrections. These later simulations have shown that an appreciable improvement of the gamma-ray energy resolution can be obtained shifting the waist of the Laser forward by 2 metre from the centre of the interaction region. In this way the peak of the gamma-ray yield is 1 metre away from the entrance of the magnetic dipole and the scattered electrons encounter a minimum of quadrupole fields in their trajectory before entering the magnet. The corresponding loss in gamma-ray flux is neglegible. The result is a gamma-ray energy resolution of 16 MeV (FWHM) or 1.1%.

Fig. 15 indicates the linear polarisation and the absolute value of the circular polarisation of the gamma-rays as a function of their relative energy.

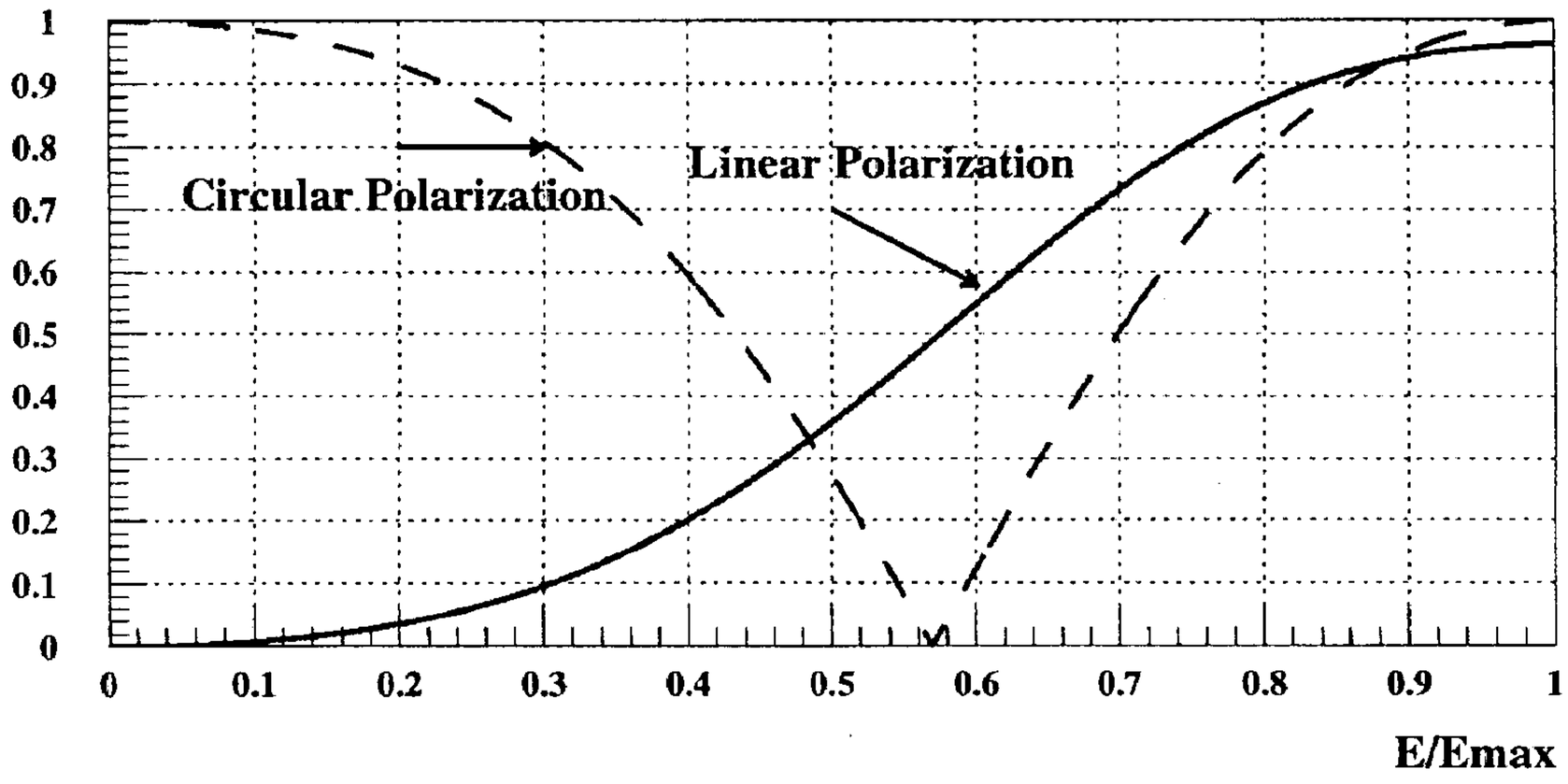

Figure 15 – The linear polarisation and the absolute value of the circular polarisation of the gamma-rays.

5.2 – External tagging

The tagging system of the LEGS facility has been extensively described elsewhere [27]. We report here the general layout and a picture of the tagging counters.

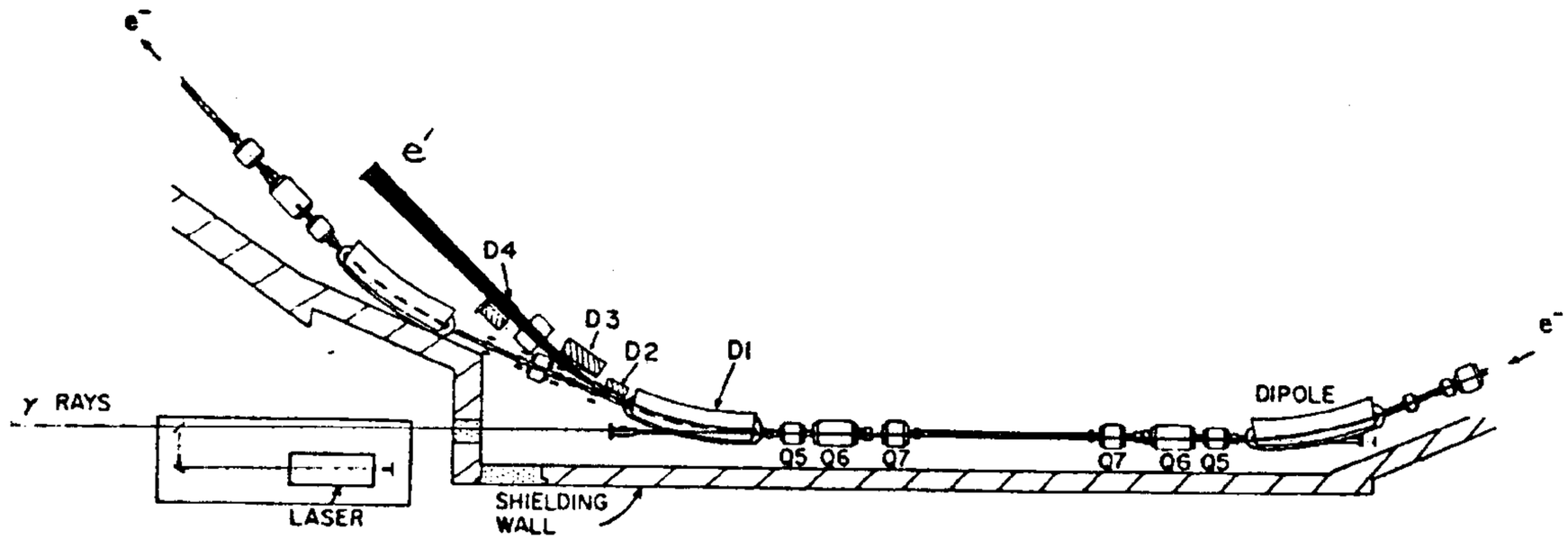

Figure 16 – The general Layout of the LEGS system [27].

Figure 17 – The Rome-built tagging detector system of the LEGS beam at Brookhaven.

6. POLARISATION

The polarisation of the gamma-rays has been calculated in the original paper of Arutyunyan and Tumanian [1]. The helicity of extremely relativistic electrons is conserved and therefore for 180° scattering there is no transfer of angular momentum from the electron to the photon. Gamma-rays moving in the direction of the electron and having the maximum energy available mantain the polarisation of the Laser light. For these gamma-rays at the top of the spectrum, the polarisation is not only complete but is also very easy to change. It suffice to change the polarisation of the Laser light. And this is true both for linear and circular polarisation.

For gamma-rays of lower energy scattered at a small angle the polarisation is less than unity but remains large over a broad energy range. The linear polarisation is larger than 0.9 down to an energy larger than 0.8 k_{max} .

For:

$k = k_{max}$ Pol = 1

$k \geq 0.8\ k_{max}$ Pol ≥ 0.9

Measuring the polarisation of high energy gamma-rays is not easy since the two most prominent QED processes, high energy Compton scattering and the creation of electron-positron pairs, show little sensitivity to the polarisation of the incoming gamma-ray.

Fortunately two hadronic reactions come to our rescue:

1. Resonant elastic scattering of polarised photons off the 15.1 MeV level of Carbon 12;
2. Coherent photoproduction of π° on Helium 4.

6.1 – $\vec{\gamma} + C^{12} \rightarrow \gamma + C^{12}$

This reaction provides the opportunity to measure the polarisation at one specific gamma-ray energy and provides also an absolute energy calibration of the beam at one point.

A first measurement was performed with a graphite target and two modest NaI(Tl) detectors placed in the plane perpendicular to the beam direction ($\theta_{Lab} = 90°$). One counter was in the vertical ($\phi = 0°$) and the other in the horizontal plane ($\phi = 90°$). The primary electron energy was adjusted to have $k_{max} = 15.1$ MeV.

The result [10] confirmed that the polarisation was complete. An energy scan around the Carbon resonant peak was performed, changing Adone's energy, and it confirmed the absolute value of the energy calibration and the energy resolution.

A second experiment was performed using a small NaI(Tl) crystal ball [24]. The counting rate of the 16 detectors situated at $\theta_{Lab} = 90°$ is reported in Fig. 18b. The dependence

$$1 + \cos 2\phi$$

on the azymuthal variable ϕ, expected for full polarisation, is confirmed.

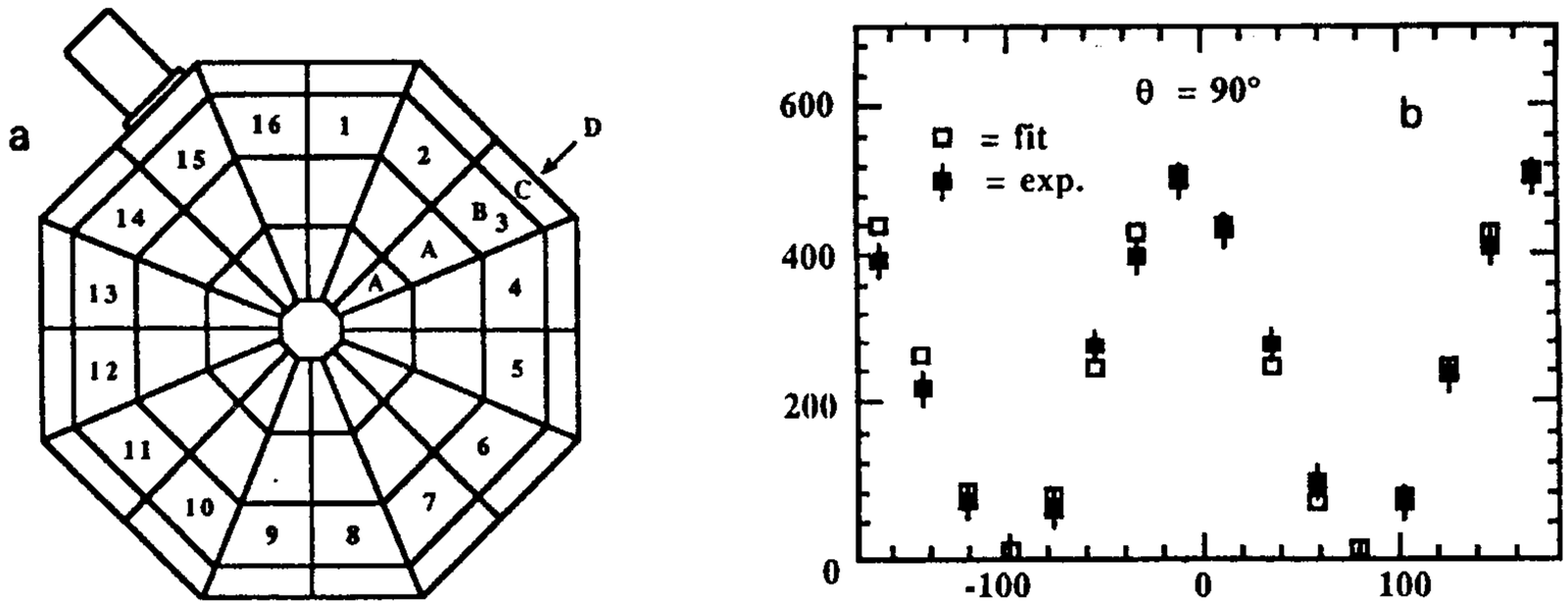

Figure 18 – (a) The layout of the small Rome NaI crystal ball in the plane perpendicular to the direction of the gamma-ray beam; (b) Azimuthal angular distribution of elastically scattered 15.1 MeV photons on ^{12}C at $\theta = 90°$.

6.2 – $\vec{\gamma}$ + $He^4 \rightarrow \pi^\circ + He^4$

The use of this reaction as a gamma-ray polarimeter has been originally suggested by Cabibbo [28]. A gamma-ray is the only particle with spin in this process and the only vectors available are:

$\vec{\varepsilon}$ the photon polarization vector
$\vec{k}$ the photon momentum
$\vec{q}$ the momentum of the pion

Therefore the only pseudo-scalar quantity (the pion is a pseudoscalar) which can be built with them is:

$$M = A\,[\vec{\varepsilon} \cdot (\vec{k} \times \vec{q})]$$

As a result the pion emission probability is zero in the direction of $\vec{\varepsilon}$ and maximum perpendicular to it.

An experiment has been performed at BNL by a LEGS-Rome-Duke collaboration to measure the coherent scattering of polarized gamma-rays on He^4 at energies between 220 and 320 MeV to study the propagation of the Δ_{33} resonance in the nucleus. The apparatus has allowed the simultaneous collection of data on the π° reaction. The data are now under analysis.

The polarisation of the outgoing gamma-ray is derived with standard Quantum Electrodynamics at low momentum trasfer and small centre of mass energy. Once trivial mistakes have been taken care of, there is no reason to believe that the calculations are not correct. Two indipendent measurements performed with different reactions, different experimental apparati, at different laboratories and at energies as far away as 15.1 and 220÷320 MeV should exaustively support our confidence in the theoretical calculations.

6.3 – Compton scattering of polarised light on polarised electrons

More recent calculations [29] [30] have taken into account also the polarisation of the incoming electron. The results exibit a small up-down asymmetry for the scattering of circular polarized photons on vertically polarised electrons at intermediate gamma-ray energies ($k \approx 0.5\ k_{max}$). This result is of interest for the study of beam dynamics in storage rings since the emission of synchrotron radiation gradually align the electron spin in the direction of the magnetic field of the bending dipoles. On the other side special machine resonances completely depolarise the electrons at fixed energies. A very high precision study of this phenomenon done on the LEP ring at CERN [31] has evidenced very small changes in the electron energy due to the deformation of the earth crust under the influence of the Moon.

Fortunately the electron polarisation does not influence in an appreciable way the polarisation of the gamma-ray.

7. – BACKGROUND

There are two source of background in a Ladon beam:

1. The low energy X-ray background produced by synchrotron radiation;
2. The high energy gamma-ray background produced by the electron Bremsstrahlung on the atoms of residual gas in the ring vacuum chamber;

7.1 – Synchrotron radiation

The synchrotron radiation of the stored electrons extends at most up to 0.5÷1 MeV. It cannot simulate nuclear events in the target. However it can produce serious problems in the experiment. They are:

a. radiation damage of optical components;
b. radiation damage of electronic components;
c. random events in the tagging counters.

Radiation damage of optical components was very serious at Ladon where we had to clean the mirror and the lens every two weeks. It is less serious at LEGS. There the vacuum is much better and an external Laser beam is used which is much less sensitive to the quality of the optical surfaces.

Also the Graal beam uses external Laser power and should have a very good vacuum in the proximity of the Beryllium mirror. This mirror is the one which should suffer the most damage since it receives directly the radiation emitted in the fringing field of the two dipoles. Fortunately the centre of the mirror is aligned with the straight section and therefore the radiation has a minimum on the optical axis on which the Laser and gamma-ray beam are aligned.

Radiation damage on solid state electronic components is a serious problems in all

accelerator tunnels. In our case the most sensitive components are the microstrip detectors of the tagger and their associated preamplifiers. Since the microstrips must be very close to the electron orbit their shielding is a difficult problem. In the Ladon beam the microstrip electronics was placed in the plane above the main orbit between two quadrupoles which provided reasonable shielding with their copper and iron. The same microstrips and electronics have been used for two years without appreciable deterioration.

Random events in the tagging counters are produced by hard X-rays which simulate the passage of an electron in the microstrips or the plastic scintillators. If the simulated electron is in the same electron bunch of a good electron then it is not clear which is to be associated with the event in the experimental apparatus and therefore which is the energy of the gamma-ray which produced the reaction. However in a fraction of these events the kinematical reconstruction allows the rejection of one alternative.

7.2 – Gamma-rays from Bremsstrahlung and beam life-time

The numbers of gamma-rays produced by the Bremmstrahlung of the electrons against the residual gas in the vacuum chamber have been calculated and measured at Ladon, LEGS and Graal detecting the electrons which have lost energy and therefore traverse the tagging scintillators. The agreement is good taking into consideration the difficulty of knowing the value of the average density and the chemical composition of the residual gas along the straight section. The vacuum gauges are located only in selected points of the ring and the mass spectrometers (Residual Gas Analysers: RGA) which give the chemical composition of the gas are used only on special occasions.

The number of Bremsstrahlung photons irradiated by an electron in a thin target is:

$$n(k)\,\Delta k = \frac{\Delta k}{k}\; t = \frac{\Delta k}{k}\,\frac{x}{X_0} = \frac{\Delta k}{k}\,\frac{P_{atm}\cdot l}{x_0}$$

$$n(k)\,\Delta k = 4.325\cdot 10^{-6}\; l\; P_{Torr}\,\frac{\Delta k}{k}$$

where

k	is the energy of the gamma-ray emitted
Δk	is the energy interval in which the radiation is emitted
t	is the thickness of the material traversed in the straight section in units of radiation length
x	is the thickness of material traversed in $g\cdot cm^{-2}$
X_0	is the radiation length of the residual gas in $g\cdot cm^{-2}$
x_0	is the radiation length of the residual gas at a temperature of 20°C and a pressure of one atmosphere (NTP) in metre. For air: $x_0 = 304.2$ m
P_{atm}	is the pressure of the residual gas in atmospheres
P_{Torr}	is the pressure of the residual gas in Tor
l	is the lenght of the straight section
l_o	is the lenght of the circumference of the ring.

In many storage rings a particle is lost if it has radiated a fraction of its energy larger than 1-2 %. Therefore the probability of loosing an electron due to Bremsstrahlung is:

$$Pr = \int_{k_{min}}^{k_{max}} n(k)dk \approx 4.3\cdot10^{-6}\ l\ P_{Torr}\ \ln\left(\frac{k_{max}}{k_{min}}\right)$$

$$Pr \approx 4.3\cdot10^{-6}\ l\ P_{Torr}\ \ln(50) \approx 1.7\cdot10^{-5}\ l\ P_{Torr}$$

The probability of loosing a particle in one revolution is:

$$P_{rev} \approx 1.7\cdot10^{-5}\ l_o\ P_{Torr}$$

and the corresponding beam life-time due to Bremsstrahlung is:

$$\tau_B = \frac{T}{P_{rev}} = 6\cdot10^4 \frac{T}{l_o\ P_{Torr}}$$

where T is the revolution time.

The effects of electron scattering and Bremsstrahlung on the residual gas are comparable and, at moderate beam current (low electron density in a bunch), they dominate the total beam lifetime (τ_T):

$$\tau_T \approx 0.5\ \tau_B$$

At higher electron density we must take into account also the Touschek effect or electron-electron intrabeam scattering within each beam bunch.

At the ESRF we have :

$l = 6$ m $\qquad l_o = 844.39$ m

$P_{Torr} \approx 10^{-9}$ Torr $\qquad T = 2.8\ \mu s$

and

$\tau_B \approx 55$ hours $\qquad \tau_T \approx 28$ hours

a value close to the one recently measured.

The number of Bremsstrahlung gamma-rays (n_B) irradiated in our interaction region in the same energy interval is:

$$n_{Bt} = N_e\ Pr$$

$$n_{Bt} \approx 1.7\cdot10^{-5} \frac{I\ l\ P_{Torr}}{e}$$

$$n_{Bt} \approx 10^5\ s^{-1}$$

where $I = 0.15$ A is the electron current in the storage ring.

This flux is between 1 and 2% of that produced by the Laser. It must be further taken into account that:

1. most of this flux is at low energy, below that detected by the tagging counters;
2. some of it is at high energy, above that detected by the tagging counters;
3. only part of it will enter the gamma ray collimator since its mean angle of aperture is of the order of $1/\gamma = m/E$;
4. this calculation must be corrected for the fact that the vacuum is not the same along all the beam orbit. The sections of the ring which have been recently opened might have a local pressure one or two orders of magnitude larger than the sections which have been properly conditioned;
5. in a tagged beam, where the energy of the gamma-rays is provided by the tagging, the Bremsstrahlung background changes only the polarisation of the beam since the Bremsstrahlung emitted around 0° is unpolarized. In most cases a contribution of the order of less than 1% can be neglected.

Bibliography

[1] F. R. Arutyunyan and V.A.Tumanian (1963). Phys. Letters **4**, 176.
Sov. Phys. Usp. **83**, 339 (1964).

[2] R. H. Milburn (1963). Phys. Rev. Letters **10,** 75.

[3] V. N. Bayer and V.A.Khoze (1969). Sov. J. Nuclear Phys. **2**, 238.

[4] O. F. Kulikov *et al.*. (1964). Phys. Letters **13**, 344.

[5] C. Bemporad *et al.* (1965). Phys. Rev. **138B**, 1546.

[6] J. Ballam *et al.* (1969). Phys. Rev. Letters **23**, 498.

[7] R. Malvano *et al.* (1967). Some considerations on the possibility of obtaining a quasi-monochromatic polarized photon beam from Laser-electron scattering in the storage ring Adone. LNF-67/48.

[8] L. Casano *et al.* (1975). Laser and Unconventional Optics Journal **55**, 3.

[9] G. Matone *et al.* (1977). Lecture Notes in Physics **62**, 149: Photonuclear Reactions II, S.Costa and C.Schaerf eds. Springer-Verlag, Berlin.
Invited contribution to the Europhysics Study Conf. on High Energy Laser and Scientific Applications, Oxford (1975).

[10] L. Federici *et al.* (1980). Nuovo Cimento **59B**, 247.

[11] D. Ivanov *et al.* (1992). Journal of Nuclear Physics, T. **55**, B 1, 3.

[12] G. Ya. Kezerashvili *et al.*, (1991). The gamma ray energy tagging spectrometer of ROKK-2 facility at VEPP-3 storage ring, Novosibirsk, preprint 91-118.

[13] A. M. Sandorfi *et al.* (1983). IEEE Trans. **NS-30**, 3083.

[14] A. M. Sandorfi *et al.*. (1989). Scattering of polarized photons at LEGS. Proceedings of the Sixth Course of the International School of Intermediate Energy Nuclear Physics, R.Bergere, S.Costa and C.Schaerf eds. World Scientific, Singapore. (BNL-42331).

[15] G. Kezerashvili *et al.*, (1994). Abstracts of the XIII International Conference Particles and Nuclei, Perugia 1993, A. Pascolini ed. World Scientific, Singapore.

[16] L. Federici *et al.* (1980). Lettere al Nuovo Cimento **27**, 339.

[17] M. Preger *et al.* (1986). Nucl. Instr. & Meth. **A249**, 299.

[18] D. Babusci *et al.*, (1990). Project Graal: the Scientific Case, Il Nuovo Cimento **103** A, 11.

[19] J. P. Bocquet *et al.* (1994). Proceedings of the XIII International Conference Particles and Nuclei, Perugia 1993, A. Pascolini ed. World Scientific, Singapore.

[20] B. E. Norum and T. P. Welch (1993). An Intense Polarized Photon Source at CEBAF Hall B.

[21] T. Scott Carmam *et al.* Production of Gamma-Rays for Nuclear Physics Using the Duke Free-Electron-Laser Facility, Technical Report, TUNL, November 1994.

[22] Calculated by J. P. Bocquet et al.. The GRAAL Green book, 1993.

[23] R. Chasman *et al.* (1975). IEEE Trans. **NS-22**, 1765.

[24] D. Babusci *et al.* (1991). Nucl. Instr. & Meth. **A305**, 19.

[25] B. Girolami, Realizzazione di uno spettrometro a coppie per il fascio Ladon, Thesis 1979, University of Rome "La Sapienza".

[26] ESRF Foundation Phase Report, 1987.

[27] C. E. Thorn *et al.* (1989). Nucl. Instr. & Meth. **A285**, 447.

[28] N. Cabibbo (1961). Phys. Rev. Lett. **7**, 386.

[29] D. B. Gustavson *et al.* (1979). Nucl. Instr. & Meth. **165**, 177.

[30] Y. S. Tsay (1993). Phys. Rev. **D 48**, 96.

[31] L. Knudsen *et al.* (1991). Phys. Lett. **B 270**, 97.